Solution Structure of a Guanine-N7-Linked Complex of the Mitomycin C Metabolite 2,7-Diaminomitosene and DNA. Basis of Sequence Selectivity[†,‡]

Gopalakrishnan Subramaniam,[§,||] Manuel M. Paz,[⊥,#] Gopinatha Suresh Kumar,[⊥,○] Arunangshu Das,[⊥] Yolanda Palom,[⊥] Cristina C. Clement,[⊥] Dinshaw J. Patel,[§] and Maria Tomasz*[,⊥]

Cellular Biochemistry and Biophysics Program, Memorial Sloan-Kettering Cancer Center, and Department of Chemistry, Hunter College, City University of New York, New York, New York 10021

Received May 11, 2001; Revised Manuscript Received June 27, 2001

ABSTRACT: 2,7-Diaminomitosene (2,7-DAM), the major metabolite of the antitumor antibiotic mitomycin C, forms DNA adducts in tumor cells. 2,7-DAM was reacted with the deoxyoligonucleotide d(GTGG-TATACCAC) under reductive alkylation conditions. The resulting DNA adduct was characterized as d(G-T-G-[M]G-T-A-T-A-C-C-A-C) (**5**), where [M]G stands for a covalently modified guanine, linked at its N7-position to C10 of the mitosene. The adducted oligonucleotide complements with itself, retaining 2-fold symmetry in the 2:1 drug−duplex complex, and provides well-resolved NMR spectra, amenable for structure determination. Adduction at the N7-position of G4 ([M]G, **4**) is characterized by a downfield shift of the G4(H8) proton and separate resonances for G4(NH_2) protons. We assigned the exchangeable and nonexchangeable proton resonances of the mitosene and the deoxyoligonucleotide in adduct duplex **5** and identified intermolecular proton−proton NOEs necessary for structural characterization. Molecular dynamics computations guided by 126 intramolecular and 48 intermolecular distance restraints were performed to define the solution structure of the 2,7-DAM−DNA complex **5**. A total of 12 structures were computed which exhibited pairwise rmsd values in the 0.54−1.42 Å range. The 2,7-DAM molecule is anchored in the major groove of DNA by its C10 covalently linked to G4(N7) and is oriented 3′ to the adducted guanine. The presence of 2,7-DAM in the major groove does not alter the overall B-DNA helical structure. Alignment in the major groove is a novel feature of the complexation of 2,7-DAM with DNA; other known major groove alkylators such as aflatoxin, possessing aromatic structural elements, form intercalated complexes. Thermal stability properties of the 2,7-DAM−DNA complex **5** were characteristic of nonintercalating guanine-N7 alkylating agents. Marked sequence selectivity of the alkylation by 2,7-DAM was observed, using a series of oligonucleotides incorporating variations of the 5′-TGGN sequence as substrates. The selectivity correlated with the sequence specificity of the negative molecular electrostatic potential of the major groove, suggesting that the alkylation selectivity of 2,7-DAM is determined by sequence-specific variation of the reactivity of the DNA. The unusual, major groove-aligned structure of the adduct **5** may account for the low cytotoxicity of 2,7-DAM.

The mitomycins are potent antitumor antibiotics produced by various strains of *Streptomyces* (*1*). Mitomycin C (MC;[1] **1**) is used clinically as a chemotherapeutic agent against several types of cancer (Chart 1; *2*). 2,7-Diaminomitosene (2,7-DAM;[1] **2**) is a major metabolite formed from MC in cells and tissues treated with the parent drug (*3*, *4*). The molecular mechanism underlying the biological and pharmacological properties of MC has attracted much attention since the discovery in 1963 that MC cross-links the complementary strands of the DNA double helix and that this represents an extremely lethal lesion in the cell (*5*). On the biochemical level complex mechanisms are involved in both the metabolic activation of MC and its subsequent cross-linking and monofunctional alkylation of DNA (*6*). Upon enzymatic or chemical reductive activation, MC forms monofunctional adducts (**S1**, **S2**) and bifunctional inter- and intrastrand cross-links (**S3**, **S4**) on DNA in the minor groove, at the exocyclic amino group of guanine residues (Chart S1, Supporting Information; *6*). The monoadducts **S1** and **S2** are formed sequence selectively at the d(C-G)·d(C-G) sequence (*7*, *8*), while the interstrand cross-link **S3** is formed at the same sequence, with absolute specificity (*9*−*11*). The structures of both monoalkylated and cross-linked MC−DNA complexes have been elucidated in our laboratories by NMR

[†] This research was supported by a grant (CA-28681) from the NIH and a Research Centers in Minority Institutions award (RR-03037) from the National Center for Research Resources of the NIH (both to M.T.) and by NIH Grant CA-46778 to D.J.P.

[‡] The coordinates of the 2,7-DAM−DNA 12-mer duplex **5** (accession number 1J01) have been deposited in the Protein Data Bank.

* Corresponding author. Phone: (212) 772-5387. Fax: (212) 650-3501. E-mail: mtomasz@hejira.hunter.cuny.edu.

[§] Memorial Sloan-Kettering Cancer Center.

[||] Current address: Department of Chemistry and Biochemistry, Queens College, Flushing, NY.

[⊥] Hunter College, CUNY.

[#] Current address: Departmento de Química Orgánica, Facultade de Ciencias, Universidade de Santiago de Compostela, Campus de Lugo, 27002 Lugo, Spain.

[○] On leave of absence from Indian Institute of Chemical Biology, Calcutta, India.

[1] Abbreviations: MC, mitomycin C; 2,7-DAM, 2,7-diaminomitosene; DMC, 10-decarbamoyl mitomycin C; MEP, molecular electrostatic potential; FAPY, formamidopyrimidine; [M]G, guanine residue substituted at N7 by 2,7-DAM, as in **4**.

10.1021/bi010965a CCC: $20.00
Published on Web 08/09/2001

Chart 1

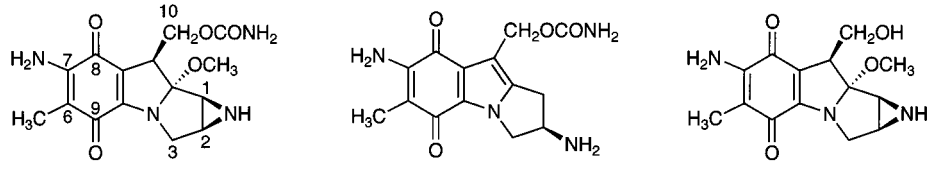

Chart 2

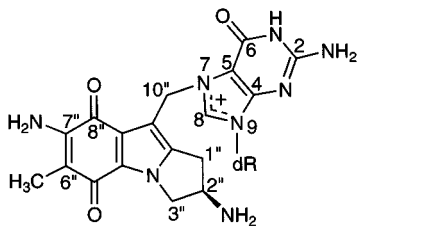

spectroscopy, combined with computational molecular modeling methods. The structures readily provided a rationale not only for the observed d(C-G)·d(C-G) specificity of the cross-link (*12*) but also for the observed preference for the same sequence in the first, monoalkylation step (*13*).

The DNA adducts of MC (**S1**−**S4**) were shown also to be formed in vivo. However, the in vivo analysis led to the unexpected discovery of an additional major adduct, **4** (Chart 2), formed side by side with the above known adducts **S1**−**S4** in cellular DNA (*14*). Adduct **4** turned out to be a guanine-N7 alkylation product of 2,7-DAM rather than an adduct of MC. Its origin in MC-treated cells was traced to the formation of 2,7-DAM from MC by a reductive pathway, followed by a second reductive activation step in situ, to 2,7-DAM hydroquinone **S5** which then alkylated DNA (Scheme S1, Supporting Information; *15*). The quinone form, 2,7-DAM itself, is unreactive. This alkylation also occurs in cells treated directly with 2,7-DAM rather than with MC (*16*).

A striking characteristic of the 2,7-DAM adduct **4** is that it is noncytotoxic, as evidenced by a lack of significant cytotoxicity of its progenitor 2,7-DAM, even under conditions which lead to high levels of intracellular formation of this DNA adduct. Although monofunctional adducts of mitomycins are expected to be less cytotoxic than cross-links, nevertheless 2,7-DAM is 2 orders of magnitude less cytotoxic than even the monofunctional decarbamoylmitomycin **3**, suggesting that the 2,7-DAM−guanine-N7 adduct **4** is unusually innocuous. Another notable difference between MC adducts and the 2,7-DAM adduct is their DNA sequence selectivity: MC adducts are selective for d(C-G)·d(C-G) steps while 2,7-DAM alkylates $d(G)_n$ tracts preferentially (*15*).

To gain further understanding of the relationship between DNA adduct structure and sequence selectivity, and perhaps even biological activity, in the mitomycin series, we determined the structure of a 2,7-DAM−DNA complex (**5**) in aqueous solution, using NMR spectroscopy and molecular dynamics methods. The self-complementary 12-mer DNA duplex **5** contains two [M]G adducts (**4**) situated four base pairs apart. The adduct is shown to be aligned in the major groove. This is novel for an aromatic natural product with a major groove-alkylating function; other known members of this class are intercalated in DNA (*17*, *18*). In addition, we report quantitative data for sequence selectivity of alkylation by 2,7-DAM of a series of 12-mer oligonucleotides, using DNA sequencing methods. The results, considered in the light of the structure of the 2,7-DAM−DNA adduct complex, suggest that the alkylation selectivity of 2,7-DAM is determined primarily by sequence-specific variation of the reactivity of DNA in the major groove.

MATERIALS AND METHODS

2,7-Diaminomitosene (**2**) was obtained by reduction of MC with H_2/PtO_2 as previously described (*4*). MC was received from Dr. D. M. Vyas, Bristol-Myers Squibb Co., Wallingford, CT. T4 polynucleotide kinase was purchased from New England Biolabs, Worcester, MA; [γ-^{32}P]ATP (10 mCi/mL, 3000 Ci/mmol) was from NEN, Boston, MA; reagents for gel electrophoresis were from Bio-Rad, Cambridge, MA.

Gel Electrophoresis. DPAGE was performed using a Hoefer Poker Face II apparatus and 36.5 × 41 cm glass plates. The loading buffer was 90% aqueous deionized formamide containing 10 mM Tris/Tris·HCl (pH 7.5) and 1 mM Na_2EDTA. The 1 × TBE buffer was 90 mM Tris/90 mM boric acid (pH 8.9) and 1.8 mM Na_2EDTA. The 20% DPAGE gels were prepared as follows: Urea (42 g) and 10 × TBE (10 mL) were added to 19:1 acrylamide/bis-(acrylamide) (40% in H_2O, 50 mL) and stirred until the urea was completely dissolved. Ammonium persulfate (10% w/v in H_2O, 350 μL) was added and the mixture filtered through Whatman no. 5 filter paper. To the resulting solution TEMED (20 μL) was added, and the gel was poured and allowed to polymerize for 1 h. Gels were equilibrated for at least 45 min before the samples were loaded.

5′-Labeling and Purification of Radiolabeled Oligonucleotides by 20% DPAGE. DNA was ^{32}P-radiolabeled at the 5′ terminus as follows: A solution of oligonucleotide (0.1 OD unit) in 20 μL of H_2O was admixed with 2.5 μL of 10 × T4PK buffer, 1 μL of [γ-^{32}P]ATP, and 2 units of T4 polynucleotide kinase (2 μL). The mixture was incubated at room temperature for 30 min and then purified by ethanol precipitation followed by purification by DPAGE. Gels (0.35 mm thickness) were run at 40 W until the xylene cyanol dye traveled 15 cm from the origin. The position of the labeled oligonucleotides was determined by autoradiography (see below). Gel slices containing the oligonucleotide were excised, and the oligonucleotide was eluted from the gel by crushing the slice with a Pasteur pipet and soaking the gel particles in 10 volumes of 0.5 M NH_4OAc, 10 mM $MgCl_2$, and 1 mM EDTA, pH 8, for 1 h. The polyacrylamide was separated by centrifugation, and the supernatant was desalted with Sep-Pak cartridges and lyophilized in a speedvac.

Alkylation of 5′-^{32}P-End-Labeled Oligonucleotides of Various Sequences by 2,7-DAM, Cleavage by Piperidine, and DPAGE. ^{32}P-Labeled self-complementary 12-mer oligonucleotides were mixed with nonradiolabeled oligonucleotide (4 mM) and 2,7-DAM (2 mM) in 0.1 M NaH_2PO_4, pH 7.8, and the mixture was hydrogenated in the presence of 100 μg of PtO_2/mmol of 2,7-DAM. PtO_2 was removed by centrifugation, and the oligonucleotide was precipitated from a 0.3 M sodium acetate, pH 5.0, solution by the addition of 7 volumes of ethanol at 0 °C, followed by storing the mixture in the freezer for 5 min and then centrifugation. Cleavage of the alkylated ^{32}P-labeled oligonucleotides by hot piperidine was carried out by heating the sample in 10% piperidine at 90 °C for 30 min, followed by lyophilization in a speedvac. The pellet was redissolved in H_2O, lyophilized again, and dissolved in gel loading buffer.

Maxam−Gilbert G-Lane. A solution of the desired amount of radiolabeled oligo was admixed with 0.2 OD unit of unlabeled oligonucleotide, diluted to 35 μL with H_2O, admixed with 10 μL of 5 × DMS buffer (0.25 M sodium cacodylate, pH 8.2, 5 mM EDTA), and cooled to 0 °C. A freshly prepared 10% solution of dimethyl sulfate in ethanol (10 μL) was added, the mixture was allowed to warm to room temperature and then incubated for 10 min, and the oligonucleotide was purified by ethanol precipitation. The pellet was heated in 100 μL of 1 M piperidine at 90 °C for 30 min, and then the solution was lyophilized in a speedvac. The pellet was redissolved in 100 μL of H_2O, lyophilized, dissolved in loading buffer, and applied to analytical 20% DPAGE, together with ^{32}P-labeled oligonucleotides modified by 2,7-DAM.

Analytical 20% DPAGE was conducted at 40 W until the xylene cyanol dye traveled 15 cm from the origin, then transferred onto sequencing filter paper, covered with Saran Wrap, and dried at 80 °C in a Bio-Rad 583 gel drier. Bands were visualized and quantitated by a Storage Phosphor Screen using Image Quant software (Applied Biosystems).

Synthesis of 2,7-DAM−Oligonucleotide Adducts Used in the NMR Study. Oligonucleotides were synthesized on an Applied Biosystems 380B automated synthesizer using cyanoethyl phosphoramidites. All reagents for the oligonucleotide synthesis were purchased from Glen Research, Sterling, VA. The resulting dimethoxytrityl-protected oligonucleotide was purified in two steps on a C4-HPLC column (Rainin Instruments Co., Woburn, MA) and desalted using G-25 Sephadex gel. The counterion was exchanged with sodium using Dowex 50-X8 cation resin.

A mixture of the self-complementary oligonucleotide d(GTGGTATACCAC) (33 μmol of nucleotide; 400 A_{260} units) and 2,7-DAM (10 μmol, 3 mg) in 10 mL of 0.1 M potassium phosphate buffer, pH 5.5, containing 0.2 mg of $Fe(NH_4)_2(SO_4)_2$, was purged with argon for 15 min and then hydrogenated in the presence of 2 mg of PtO_2 by bubbling H_2 gas through the solution for 17 min at room temperature. A mild color change from dark purple to light grayish purple was observed. The argon atmosphere was maintained for 1 h. The PtO_2 was then removed by filtration (0.2 μm filter), and the reaction mixture was dialyzed in the cold room four times, with 4 L of 10 mM sodium phosphate, pH 6.8, for 6 h each. The solution was lyophilized and subjected to semipreparative reverse-phase C18-HPLC, using a semipreparative column (2.5 × 10 cm, Keystone) and a gradient elution system of 0−25% methanol in 20 mM sodium phosphate, pH 6.8, in 40 min, at a 3 mL/min flow rate. The adduct-containing fraction was eluted after the parent oligonucleotide, as recognized by its absorbance at 310 nm, and lyophilized. Excess salt was removed by dialysis. The yield of the modified 12-mer (**5**) was 20% (80 A_{260} units). Synthesis of adduct **6** was carried out by the analogous procedure using the 10-mer d(GTGGTACCAC) duplex as starting material.

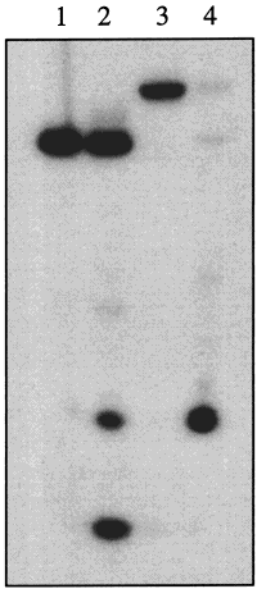

FIGURE 1: Determination of the position of the 2,7-DAM adduct in the oligonucleotide **5** used for the NMR study. The parent oligonucleotide 5′-GTGGTATACCAC and the HPLC-purified modified oligonucleotide (top strand of **5**) were ^{32}P-labeled at their 5′-terminal positions and analyzed by DPAGE. Both showed one major band, which was isolated from the gel (not shown). The isolated ^{32}P-labeled oligonucleotides were then used for the analysis of the position of the 2,7-DAM adduct in the modified oligonucleotide. Lane 1: parent oligonucleotide. Lane 2: G-specific cleavage of the parent oligonucleotide with dimethyl sulfate and hot piperidine. Lane 3: 2,7-DAM-modified oligonucleotide **5**. Lane 4: same as lane 3 but heated in 1 M piperidine.

*Verification of Structure **5***. (i) Adduct **5** was digested by snake venom diesterase and alkaline phosphatase by previously described methods (*19*). The digest was heated at 90 °C for 1 h to hydrolyze **4** to the deribosylated guanine adduct **S7** (Scheme S2, Supporting Information), and the mixture was analyzed by HPLC. Molar ratios of the individual nucleosides and the adduct **S7** were determined from HPLC peak areas and corresponding molar extinction coefficients at 254 nm, as previously described (*19*). Good agreement was obtained between the theoretical and experimental molar ratios. (ii) Determining the position of the adduct in the modified dodecamer **5** was accomplished by 5′-^{32}P-labeling of the unmodified parent and modified oligonucleotide **5**. The labeled parent was used to produce a Maxam−Gilbert G-lane, and the labeled modified oligo **5** was cleaved by hot piperidine; both were analyzed by DPAGE. The cleavage pattern showed clearly that the position of the 2,7-DAM−guanine-N7 adduct was at G4 (Figure 1).

UV Spectroscopy and Melting Studies. Oligonucleotide concentrations were determined using the following formula: ϵ_{260}(strand) = number of purines × 14 000 + number of pyrimidines × 7000. In the case of the alkylated

oligonucleotide a correction for ϵ_{260}(strand) was done by adding 5189 (ϵ_{260} of 2,7-DAM). ϵ_{260}(duplex) was assumed as equal to $2 \times \epsilon_{260}$(strand). The ϵ_{260} for the duplex of the nonalkylated oligonucleotide was 252 000 M^{-1} cm^{-1} while the ϵ_{260} for the alkylated duplex was 262 378 M^{-1} cm^{-1}. The concentration of the oligonucleotide (strand) was 2.2 μM in all melting experiments.

Thermal melting curves at 260 nm were determined using a Cary-3 spectrophotometer. Temperature control was obtained through a jacketed cell holder connected to a water bath and controlled by the software of the Cary-3. The samples were heated gradually in stoppered cuvettes of 1 cm path length. The temperature range was 20−85 °C. The data were acquired with 0.8 °C increments/min at each 15 s, such that a total of 260 data points were acquired for each sample. The melting curve data were fitted by sigma plot nonlinear regression analysis to a sigmoid curve. Three independent experiments were carried out on each sample, and the resulting T_ms were averaged. Immediately prior to analysis the samples were incubated at 60 °C for 3 min and then slowly cooled at room temperature to provide the annealing.

Thermodynamic Analysis of the Melting Curves. Melting temperature T_m and the thermodynamic parameters that characterize the helix−coil transition of the DNA duplexes were determined by employing the built-in Cary-3 software. The method of choice for the calculation of the thermodynamic parameters was direct application of the van't Hoff equation (*20*).

NMR Experiments. For NMR experiments, all samples were dissolved in 0.5 mL of aqueous buffer (10 mM sodium phosphate, 0.1 M sodium chloride, 1 mM EDTA, pH 6.8) and lyophilized. For experiments in H_2O, the samples were dissolved in 10% D_2O. For experiments in D_2O, the samples were relyophilized three times in 99.8% D_2O and finally dissolved in 99.96% D_2O.

All NMR experiments were recorded on Varian Unityplus 600 or 500 MHz NMR spectrometers. All data sets were processed using vnmr (Varian Instruments) or Felix (MSI) software. The solvent signal was suppressed with presaturation in D_2O samples and shaped pulse in H_2O samples. Two-dimensional NOESY data sets of the self-complementary d(G-T-G-[M]G-T-A-T-A-C-C-A-C) (**5**) and d(G-T-G-[M]G-T-A-C-C-A-C)·d(G-T-G-G-T-A-C-C-A-C) (**6**) duplexes were recorded in D_2O at 5 °C with a mixing time of 250 ms. Continuous low-power irradiation of the residual HOD signal was applied during the recycle time for all spectra in D_2O. The spectral width was 9 ppm, and 2048 complex data points and 64 transients were acquired for each fid in t_2. A HOHAHA (80 ms mixing time) at 5 °C and phase-sensitive COSY spectra at 5 and 30 °C were also recorded on adduct **5** in D_2O buffer.

Two-dimensional data sets on the above duplexes were also recorded in H_2O at 0 °C using jump−return as the detection pulse (*21*). The delay during jump−return was 52 μs to optimize the excitation of the imino resonances. The relaxation time was 1.7 s, and the mixing time was 150 ms.

A proton-decoupled ^{31}P NMR spectrum was obtained on the self-complementary d(G-T-G-[M]G-T-A-T-A-C-C-A-C) duplex **5** in the temperature range of 5−30 °C with 1024 transients, sweep width of 10 ppm, and at a proton frequency of 500 MHz. The phosphorus peaks were broad and restricted to the −4.0 to −5.0 ppm range.

Interproton Distance and Dihedral Restraints. For distance measurements on the self-complementary d(G-T-G-[M]G-T-A-T-A-C-C-A-C) duplex **5**, a set of NOESY spectra were collected using the Holboken−States method with 50, 100, 150, and 250 ms mixing times at 5 °C with a sweep width of 9 ppm, 2048 complex data points, and 64 transients for each fid in t_2. Both time−domain data sets were multiplied by a 90° phase-shifted sine-bell window function. The first fid was multiplied by 0.5 to avoid t_1 ridge artifacts. The initial slopes were computed, and approximate distances between proton pairs were estimated using the two-spin approximation and calibration against buildups for fixed interproton distances. For all nonexchangeable proton pairs except those which involve CH_3 groups, the slopes were compared to the average of the slopes of C9 and C10 H5-H6 cross-peak slopes which were given a reference distance of 2.5 Å. For those cross-peaks involving methyl protons, the slopes of the three thymidine CH_3-H6 were averaged and referenced to 2.9 Å fixed distance. For those NOEs involving exchangeable protons, the distances were approximately estimated from the relative strength of the cross-peaks in the NOESY spectrum in H_2O recorded at a mixing time of 150 ms. Medium cross-peaks were given a bound of 2.0−4.0 Å, while weak cross-peaks were given a bound of 3.0−5.0 Å.

Dihedral angle restraints defining the sugar pucker and specific backbone torsion angles were restricted for residues other than those centered about the [M]G4 adduct site in duplex **5**.

Structure Calculations. Two starting structures were built for the complex using A-DNA and B-DNA helices as starting points. The 2,7-DAM and the DNA helix were built in Insight (MSI) using standard templates, and the 2,7-DAM was visually positioned near the G4(N7) in the major groove. Covalent bonding between C10 of 2,7-DAM and N7 of G4 was specified in the topology file. The parameters for 2,7-DAM were obtained by inference from mitomycin C (*13*). Molecular dynamics calculations were done using a Silicon Graphics Challenge computer. The X-PLOR (A. Brunger, Yale University) based restrained molecular dynamics (MD) calculations for each structure were carried out in two cycles with different seeds using the simulated annealing protocol and the CHARMM force field with reduced phosphate charges. Watson−Crick base pairing alignments on all observed hydrogen bonds were maintained throughout the dynamics by imposing hydrogen-bonding distance restraints (±0.125 Å) between the two strands. A total of 48 dihedral restraints on residues other than those centered about the adduction site were restricted to canonical B-form (±35°) with a force constant of 50 kcal during the MD simulation. Each cycle of restrained MD simulation was initially carried out at 300 K with a force constant of 60 kcal mol^{-1} $Å^{-2}$ for hydrogen-bonding restraints and 1 kcal for other experimentally observed distance restraints and subjected to 1500 cycles of energy minimization. The force constants for experimentally observed NOEs were then scaled to 30 kcal mol^{-1} $Å^{-2}$, and a high-temperature dynamics was carried out at 1000 K for 2.0 ps (time step of 0.1 fs). The system was gradually cooled to 300 K over 1.7 ps (time step of 0.4 fs) with retention of full scale of restraints. This was followed by 4.8 ps (time step of 0.6 fs) of molecular dynamics at 300 K.

Chart 3

G1 - T2 - G3 - [M]G4 - T5 - A6 - T7 - A8 - C9 - C10 - A11 - C12

C12 - A11 - C10 - C9 - A8 - T7 - A6 - T5 - [M]G4 - G3 - T2 - G1

5

Self-complementary dodecamer duplex containing two [M]G adducts.

G1 - T2 - G3 - [M]G4 - T5 - A6 - C7 - C8 - A9 - C10

C20 - A19 - C18 - C17 - A16 - T15 - G14 - G13 - T12 - G11

6

Decamer duplex containing one [M]G adduct.

The coordinates during the last 1.0 ps of dynamics were averaged, and these averaged coordinates were subjected to 500 cycles of energy minimization with noncrystallographic symmetry restraint.

RESULTS

Synthesis of 2,7-Diaminomitosene Adducts with d(G-T-G-G-T-A-T-A-C-C-A-C) and with d(G-T-G-G-T-A-C-C-A-C) (*Chart 3*). We synthesized the 2,7-diaminomitosene adduct with d(G-T-G-G-T-A-T-A-C-C-A-C) and purified it using reverse-phase C18-HPLC. The G4-position as the adduct site was established as described in the Materials and Methods section and is shown in Figure 1. This adduct designated as d(G-T-G-[M]G-T-A-T-A-C-C-A-C) (**5**) complemented with itself as observed by imino proton resonances in the NMR spectrum run in H_2O (Figure S1a, Supporting Information). The lower homologue oligonucleotide decamer d(G-T-G-G-T-A-C-C-A-C) also formed an adduct with 2,7-DAM, designated as d(G-T-G-[M]G-T-A-C-C-A-C). However, this adduct did not form a symmetrical duplex analogous to duplex **5**. Nevertheless, it hybridized readily with the unsubstituted complementary strand to give the decamer heteroduplex **6** as observed by the proton NMR spectrum run in H_2O (data not shown). The symmetry of adduct **5** reduced spectral crowding of the exchangeable protons compared to adduct **6** and hence was chosen for detailed structural studies. It is important to note that adduct **6** exhibited spectral features similar to those of adduct **5**, which were very useful in cross-checking spectral assignments and NOE patterns.

NMR Spectral Quality. The 8.0−14.0 ppm exchangeable (Figure S1a, Supporting Information) and the 0.0−8.5 ppm nonexchangeable (Figure S1b, Supporting Information) proton NMR spectra of the d(G-T-G-[M]G-T-A-T-A-C-C-A-C) duplex **5** establish that the adduct duplex exists predominantly in a single conformation in aqueous solution. The H8 proton of [M]G4 resonates at 8.43 ppm, and its downfield shift is consistent with protonation at the N7 position of the guanine ring on adduct formation (*22*).

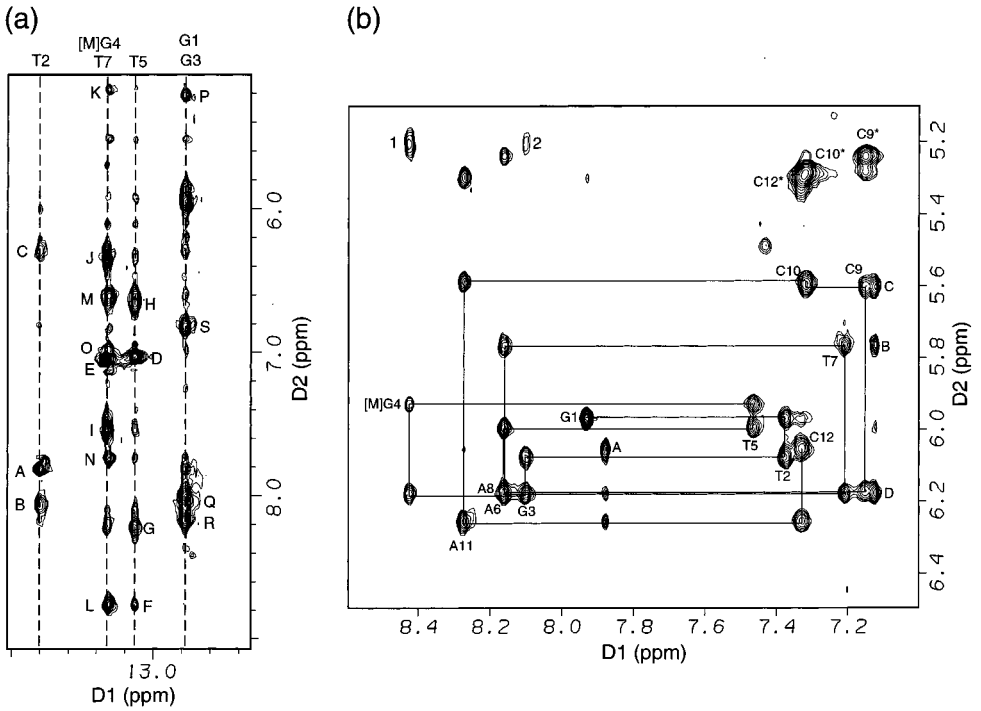

FIGURE 2: (a) Expanded NOESY contour plot (150 ms mixing time) showing NOE connectivities between the imino protons and the base and amino protons (5.0−9.0 ppm) for the self-complementary d(G1-T2-G3-[M]G4-T5-A6-T7-A8-C9-C10-A11-C12) adduct duplex **5** in H_2O buffer, pH 6.8 at 0 °C. Peaks labeled A−S are assigned as follows: (A) T2(N3H)-A11(H2); (B) T2(N3H)-A11(NH_2-6b); (C) T2(N3H)-A11(NH_2-6e); (D) T5(N3H)-A8(H2); (E) T7(N3H)-A6(H2); (F) T5(N3H)-[M]G4(NH_2-2b); (G) T5(N3H)-A8(NH_2-6b); (H) T5(N3H)-A8(NH_2-6e); (I) T7(N3H)-A6(NH_2-6b); (J) T7(N3H)-A6(NH_2-6e); (K) [M]G4(N1H)-C9(H5); (L) [M]G4(N1H)-[M]G4(NH_2-2b); (M) [M]G4(N1H)-[M]G4(NH_2-2e); (N) [M]G4(N1H)-C9(NH_2-4b); (O) [M]G4(N1H)-C9(NH_2-4e); (P) G1(N1H)-C12(H5) and G3(N1H)-C10(H5); (Q) G1(N1H)-C12(NH_2-4b); (R) G3(N1H)-C10(NH_2-4b); (S) G1(N1H)-C12(NH_2-4e) and G3(N1H)-C10(NH_2-4e). (b) Expanded NOESY contour plot (250 ms mixing time) showing NOE connectivities between the base protons and anomeric protons for the self-complementary d(G1-T2-G3-[M]G4-T5-A6-T7-A8-C9-C10-A11-C12) adduct duplex **5** in D_2O buffer, pH 6.8 at 5 °C. The intraresidue base-H1′ NOE cross-peaks are labeled. The cytosine H5-H6 NOEs are marked with asterisks. The intermolecular NOEs marked 1 and 2 are assigned as follows: (1) [M]G4(H8)-[M]10″H_b; (2) G3(H8)-[M]10″H_b. Peaks marked A−D are intramolecular NOEs and are assigned as follows: (A) A11(H2)-C12(H1′); (B) A6(H2)-T7(H1′); (C) A8(H2)-C9(H1′); (D) A6(H2)-A6(H1′), A8(H2)-A8(H1′).

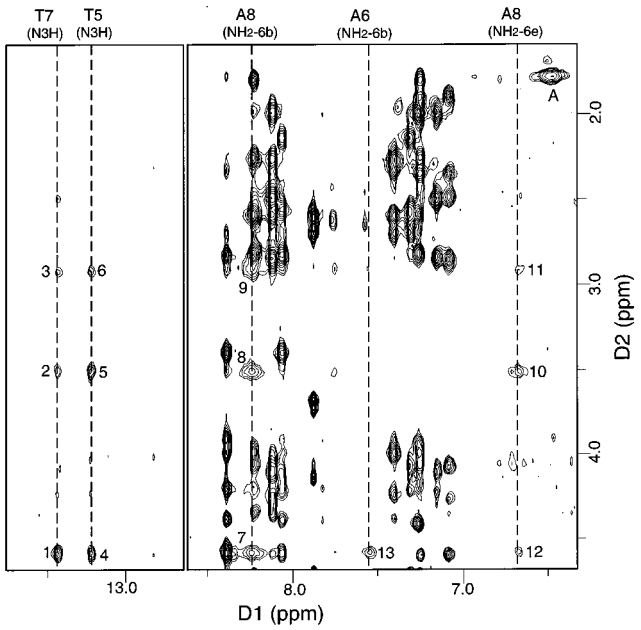

FIGURE 3: Expanded NOESY contour plot (150 ms mixing time) showing NOE connectivities between the imino protons and other protons in the 1.6−4.6 ppm region for the self-complementary d(G1-T2-G3-[M]G4-T5-A6-T7-A8-C9-C10-A11-C12) adduct duplex **5** in H_2O buffer, pH 6.8 at 0 °C. Peaks labeled 1−13 are intermolecular NOEs and are assigned as follows: (1) T7(N3H)-[M]2″H; (2) T7(N3H)-[M]1″H_a; (3) T7(N3H)-[M]1″H_b; (4) T5(N3H)-[M]2″H; (5) T5(N3H)-[M]1″H_a; (6) T5(N3H)-[M]1″H_b; (7) A8(NH_2-6b)-[M]2″H; (8) A8(NH_2-6b)-[M]H1″a; (9) A8(NH_2-6b)-[M]H1″b; (10) A8(NH_2-6e)-[M]1″H_a; (11) A8(NH_2-6e)-[M]1″H_b; (12) A8(NH_2-6e)-[M]2″H; (13) A6(NH_2-6b)-[M]2″H. The peak marked A is the intramolecular NOE between [M]7″NH_2 and [M]6″CH_3.

Previous studies have shown that N7-modified guanine adducts are susceptible to deglycosylation (*17*, *22*), and hence all NMR studies were undertaken on recently prepared samples buffered to pH 6.8 and data collected as rapidly as possible at temperatures at or below 5 °C.

Exchangeable Proton Assignments. We observe four resolved imino proton resonances between 12.7 and 13.4 ppm in the spectrum of adduct duplex **5** (Figure S1a, Supporting Information) in H_2O buffer at 0 °C. Two of these have twice the intensity as the others, resulting in a total of six imino protons, consistent with the expected number for a self-complementary 12-mer duplex. These imino protons have been assigned following analysis of a 150 ms mixing time NOESY spectrum in H_2O buffer at 0 °C. The labeled cross-peaks in the expanded NOESY contour plot in Figure 3 are assigned in the caption to the figure. The imino proton of modified [M]G4 and T7 are superpositioned at 13.33 ppm while those of terminal G1 and G3 are superpositioned at 12.79 ppm. The observation of cross- strand NOEs between the imino proton of [M]G4 and the amino protons of C9 (peaks N and O, Figure 2a) are consistent with Watson−Crick [M]G4·C9 pair formation. In addition, cross-strand NOEs between the imino proton of G3 and the amino protons of C10 (peaks R and S, Figure 3) and cross-strand NOEs between the imino proton of T5 and the H2 proton of A8 (peak D, Figure 2a) are consistent with the formation of Watson−Crick G3·C10 and T5·A8 pairs flanking the modification site.

The imino proton of [M]G4 resonating at 13.33 ppm is downfield from the other guanine imino protons and reflects the N7 protonation of the modified guanine ring. Protonation of the [M]G4 ring also results in separate resonances for its 2-NH_2 protons which resonate at 8.76 and 6.61 ppm. We observe the 7-NH_2 (6.48 ppm) but not the 2-NH_2 protons of the 2,7-DAM moiety in the NMR spectrum of adduct duplex **5**. The 7-NH_2 protons at 6.48 ppm are broad and have been assigned by through-space connectivities to the 6-CH_3 protons.

Table 1: Chemical Shifts and Intermolecular NOEs for the Protons of the 2,7-DAM Residue [M], **4**, in the Self-Complementary d(G1-T2-G3-[M]G4-T5-A6-T7-A8-C9-C10-A11-C12) Adduct Duplex **5**

proton	δ (ppm)	intermolecular NOEs
1″CH_2	2.99, 3.56	T5(N3H), T5(CH_3), A8(NH_2-6b/e), T7(N3H)
2″H	4.63	T5(N3H), T5(CH_3), A8(NH_2-6b/e), A6(NH_2-6b/e), T7(N3H), T7(CH_3)
3″CH_2	3.57, 4.63	T5(CH_3), T7(CH_3)
6″CH_3	1.84	T5(CH_3)
7″NH_2	6.48	
10″CH_2	4.63, 5.21	G3(H8), [M]G4(H8), T5(CH_3)

Nonexchangeable Proton Assignments. The nonexchangeable base and sugar protons in adduct duplex **5** have been assigned following analysis of NOESY and COSY data sets in D_2O solution at 5 °C. The base to sugar H1′ proton connectivities are outlined in the expanded 250 ms mixing time NOESY spectrum in Figure 2b. We are able to trace the NOE connectivities between the base and their own and 5′-linked sugar H1′ protons along the entire length of the adduct duplex. The H8 proton of [M]G4 resonates at 8.43 ppm, and its downfield shift is consistent with N7 protonation of the guanine ring. The CH_3 group of T5 resonates at 0.44 ppm, which is to high field of the unperturbed CH_3 region. An unusual pattern of NOEs is observed for the H8 proton of [M]G4, which shows weak NOEs to its own sugar H2′,2″ protons but strong NOEs to the sugar H2′,2″ protons of its flanking G3 residue (Figure S2, Supporting Information). The exchangeable and nonexchangeable nucleic acid proton chemical shifts for adduct duplex **5** are listed in Table S1 (Supporting Information).

The 2,7-DAM protons in adduct duplex **5** were assigned following analysis of through-bond (Figure S3, Supporting Information) and through-space connectivities. The methylene protons at positions 1″, 3″, and 10″ have been differentiated on the basis of their chemical shift patterns. The downfield-shifted 4.63 and 5.21 ppm methylene protons were assigned to the 10″-position which is flanked by a deshielding nitrogen atom and an olefinic ring. The methylene proton resonances at 3.57 and 4.63 ppm were assigned to the 3″-position, which is flanked by a deshielding nitrogen. The 2.99 and 3.56 ppm methylene protons, which resonate at highest field, were assigned to the 1″-position, which is flanked by a double bond. The proton at 4.63 ppm, which exhibits NOEs to the 1″ and 3″ methylene protons, is assigned to the proton at the 2″-position. The exchangeable and nonexchangeable 2,7-DAM proton chemical shifts in the adduct duplex **5** are listed in Table 1.

Intermolecular NOEs. We have identified a set of intermolecular NOEs which have been critical for defining the alignment of the 2,7-DAM along the DNA in adduct duplex **5** (Table 1). The protons along the 1″-2″-3″ edge and 6″-position of 2,7-DAM exhibit NOEs primarily to the adjacent

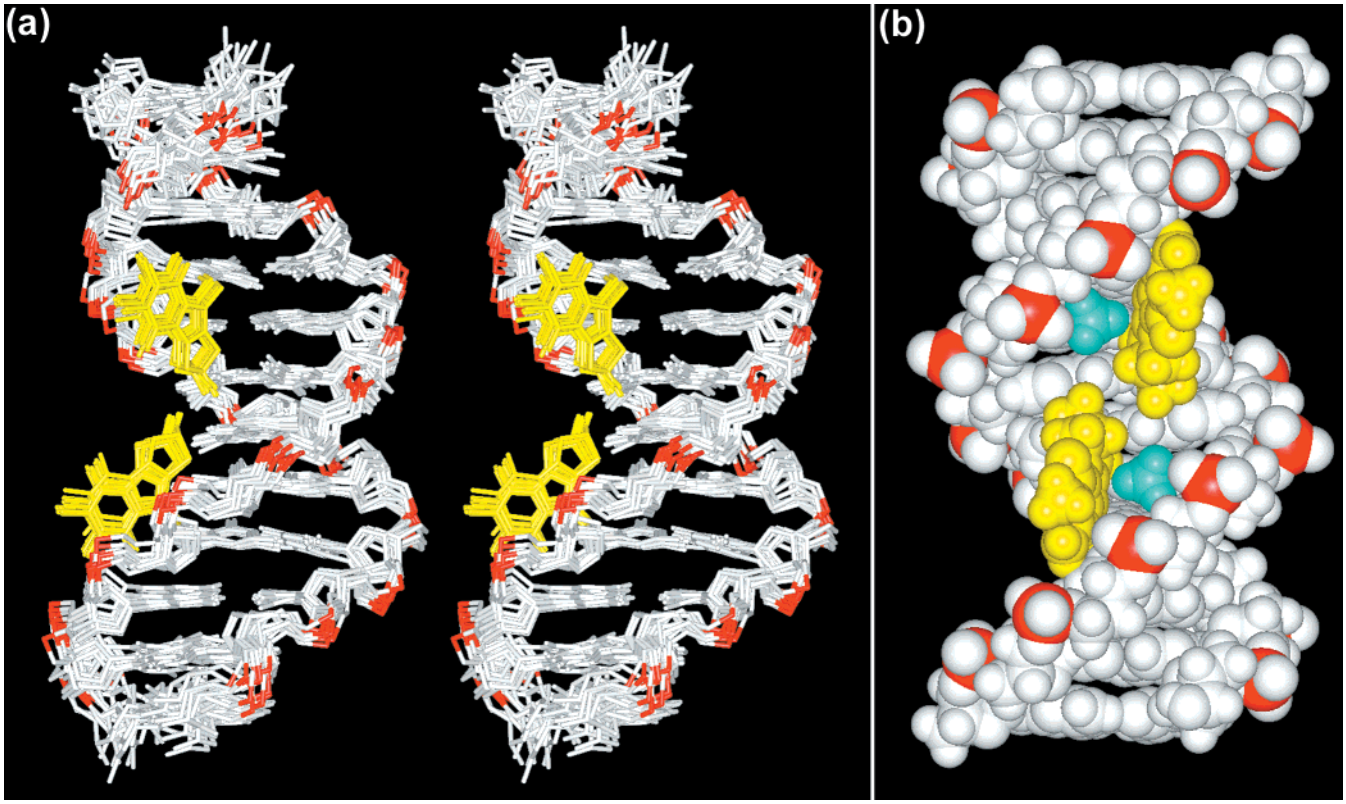

FIGURE 4: (a) Stick stereoviews of 12 distance-refined structures of the self-complementary d(G1-T2-G3-[M]G4-T5-A6-T7-A8-C9-C10-A11-C12) adduct duplex **5**. The 2,7-DAM moiety is shown in yellow, and the phosphorus atoms are shown in red. (b) Space-filling view looking into the major groove of the structure of the self-complementary d(G1-T2-G3-[M]G4-T5-A6-T7-A8-C9-C10-A11-C12) adduct duplex **5**. The 2,7-DAM moiety is in yellow, and the T5 methyl group is in cyan.

T5·A8 base pair and next nearest neighbor T7, directed in the 3′ direction along the modified strand. These intermolecular NOEs are labeled numerically in Figure 4 with the assignments listed in the figure caption. By contrast, the methylene protons at 10″ exhibit NOEs within the G3-[M]-G4-T5 segment of the modified strand. The intermolecular NOEs between the 10″ methylene protons of 2,7-DAM and the H8 protons of [M]G4 and G3 are labeled peaks 1 and 2 in Figure 2b. The same pattern of intermolecular NOEs have also been observed for adduct duplex **6**, which contains one bound 2,7-DAM molecule, and for adduct duplex **5**, which contains two bound 2,7-DAM molecules on partner strands separated by four A·T base pairs.

Distance-Restrained Molecular Dynamic Computations. The distance-restrained molecular dynamics computations on the 2-fold symmetric adduct duplex **5** were guided by 126 intramolecular and 48 intermolecular restraints obtained from NOESY data sets in D_2O collected at four mixing times and in H_2O at one mixing time. Dihedral (48 in total) and hydrogen-bonding (30 in total) restraints were also used to guide the computations. The dynamics protocols are outlined in the Materials and Methods section. A total of 12 low-energy distance-refined structures are shown in stereo in Figure 4a, with the covalently bound 2,7-DAM highlighted in yellow. The pairwise heavy atom rmsd values between refined structures range between 0.54 and 1.42 Å (Table 2).

Structural Features. A stereoview of superpositioned distance-refined solution structures of the d(G-T-G-[M]G-T-A-T-A-C-C-A-C) adduct duplex **5** is plotted in Figure 4a. The solution structure of adduct duplex **5** is well-defined except for the terminal base pairs (Figure 4a). The DNA

Table 2: NMR Refinement Statistics for d(G-T-G-[M]G-T-A-T-A-C-C-A-C) Adduct Duplex **5**

NMR distance restraints[a]	
total no. of DNA distance restraints	156
no. of intramolecular DNA distance restraints	126
no. of hydrogen-bonding distance restraints	30
total no. of 2,7-DAM distance restraints	0
total no. of intermolecular distance restraints	48
exchangeable distance restraints	18
nonexchangeable distance restraints	30
dihedral restraints[b]	
total no. of dihedral restraints	48
structural statistics	
NOE violations	
number >0.2 Å	6−10
rmsd of violations	0.059−0.067
deviations from ideal covalent geometry	
bond length (Å)	0.008−0.010
bond angle (deg)	3.74−4.07
impropers (deg)	0.298−0.463
pairwise rmsd for the 12 final structures	0.54−1.42

[a] NMR distance restraints are for the entire adduct. [b] Dihedral restraints defining sugar pucker and specific backbone torsion angles were restricted for residues other than those centered about the [M]G4 adduct site.

retains B-form geometry with *anti* glycosidic torsion angles and C2′-*endo* sugar pucker geometries, with the exception of [M]G4, which adopts a C3′-*endo* sugar pucker (the H1′-H2′ cross-peak of [M]G4 is absent in the COSY contour plot; Figure S4b, Supporting Information). The base pair twist (Figure S5e, Supporting Information) and rise (Figure S5f, Supporting Information) vary with step, both at and adjacent to the [M]G4 adduct site, suggestive of adduct-induced structural perturbations that extend into the central A·T rich

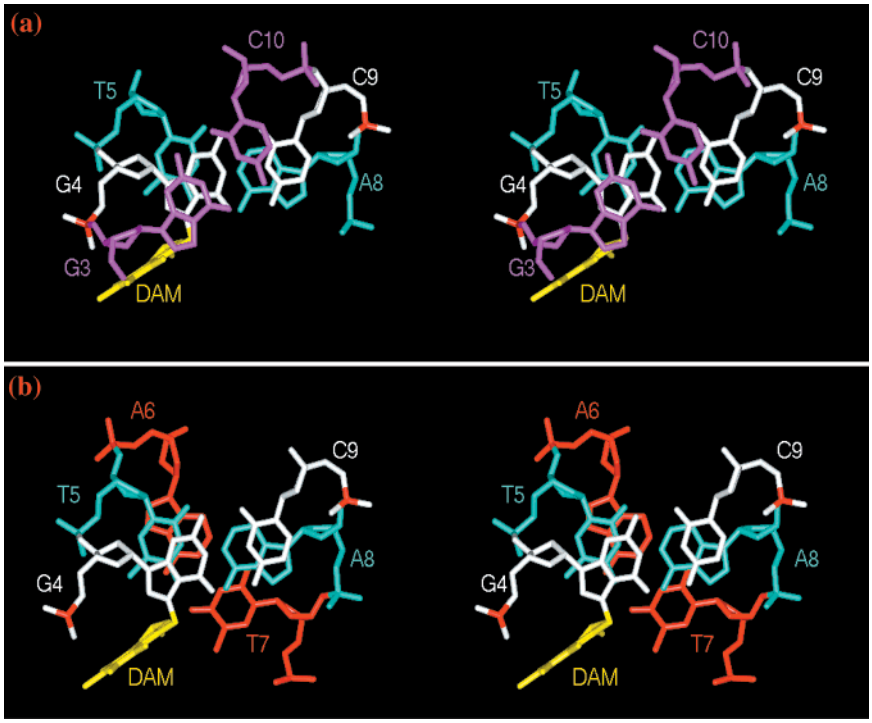

FIGURE 5: Stick stereoviews of the overlap geometries in a representative refined structure of the self-complementary d(G1-T2-G3-[M]-G4-T5-A6-T7-A8-C9-C10-A11-C12) adduct duplex **5**. The top view shows the overlap between G3·C10, [M]G4·C9, and T5·A8 base pairs while the bottom view shows the overlap between the [M]G4·C9, T5·A8, and A6·T7 base pairs. Note that the 2,7-DAM ring stacks on the CH_3 group of the T5 base next to the adduct site and does not have any interactions with the partner strand. It is also evident that base stacking in the partner strand is reduced while stacking in the adduct strand is maintained.

Table 3: Effect of the 2,7-DAM−Guanine-N7 Adduct **4** in the Self-Complementary d(GTGGTATACCAC) Adduct Duplex **5** on Thermal and Thermodynamical Duplex Stability, Spectroscopically Determined T_m, and Calculated Changes of the van't Hoff Transition Enthalpy ($\Delta H°$), Entropy ($\Delta S°$), and Free Energy ($\Delta G_{25}°$) for the Coil-to-Helix Transition[a]

oligonucleotide	T_m (°C)	$\Delta H°$ (kcal/mol)	$\Delta S°$ (cal mol^{-1} K^{-1})	$\Delta G°_{25°C}$ (kcal/mol)
d(GTGGTATACCAC)	51.0 ± 0.4	−49.2 ± 2.0	−125.7 ± 5.9	−11.7 ± 0.2
d(GTG[M]GTATACCAC)[b] (**5**)	42.1 ± 0.4	−78.6 ± 6.1	−223.2 ± 1.9	−12.1 ± 0.3

[a] The thermodynamic parameters were extracted from the melting curves (Figure S6, Supplementary Information) by direct application of the van't Hoff equation (*20*) using the Cary-3 software. [b] [M]G denotes the adducted guanine residue.

tetranucleotide segment in adduct duplex **5**. The 2,7-DAM is positioned closer to the backbone of the adducted strand and is aligned approximately parallel to the helix axis (Table S2, Supporting Information), and its aromatic ring stacks on top of the CH_3 group of T5 (Figure 4b). The stacking pattern between the [M]G4·C9 pair and two base pairs in either direction is shown in Figure 5. Further, the stacking of the CH_3 group of T5 over the 2,7-DAM ring (Figure 4b) restricts the orientation of the DAM ring to being approximately parallel to the helix axis (Figure 4b) rather than parallel to the sugar−phosphate backbone.

Melting Studies and Thermodynamic Analysis of the Melting Curves. One potential problem that arises in the case of guanyl-N7 adducts is sensitivity toward thermal depurination (*23*). To minimize the experimental artifacts due to this effect, melting experiments were conducted such that the temperature increase was relatively fast (0.80 °C min^{-1}) to avoid excessive incubation at each temperature step, although in a range acceptable for short oligonucleotide duplexes. Figure S6 (Supporting Information) presents the melting curves of the control duplex and 2,7-DAM-adducted duplex **5**. Depurination was not significant, as seen by their complete reversibility and by HPLC analysis of the melted sample (data not shown). The melting temperatures are lower for the alkylated duplex **5** (two adducts per duplex) as compared with the control, with $\Delta T_m = 8.90 \pm 0.70$ °C. The reduction in the thermal stability of other nonintercalating N7-guanyl adducts is in the range of ∼11 °C (*24*), which is not far from that found for the 2,7-DAM adduct. The hyperchromicity for the nonadducted duplex was 15.5% while that for the adducted duplex **5** was 7.6%. The lower hyperchromicity of the adducted duplex could be due to helical perturbations centered about the adducted bases.

The shape of the melting curves is compatible with a two-state cooperative transition between the helix and the coil states both for the nonalkylated and for the adducted duplexes The results of van't Hoff analysis of the melting curves based on this assumption are presented in Table 3. The transition enthalpy for the adducted duplex **5** facilitates duplex formation by −29.4 kcal/mol over that of the parent counterpart, while the transition entropy is less favorable, as a difference of −98 cal mol^{-1} K^{-1} was observed. In the case of other major groove-located guanyl-N7 adducts the thermodynamic analysis of melting curves also showed that enthalpy of the alkylated duplex is more favorable, while the entropy is less favorable, suggesting that the decrease in the thermal stability

of the adducted duplex is due to the entropic component (*24*, *25*). It has been also speculated that the more favorable coil-to-helix transition enthalpy of the adducted duplex may be due to the positive charge imposed on the imidazole ring by N7-guanine alkylation (*24*). The ΔG of the coil-to-helix transition of the adducted duplex is only slightly lower than that of the parent duplex ($\Delta\Delta G^{\circ}_{25^{\circ}C} = -0.3$ kcal/mol); this is also analogous to the other G-N7 alkylated oligonucleotides (*24*, *25*).

DNA Sequence Selectivity of the 2,7-DAM−Guanine-N7 Adduct in a Series of 5′-GGN-Containing 12-mer Oligonucleotides. ^{32}P-Labeled oligonucleotides were alkylated by 2,7-DAM under H_2/PtO_2 reductive activation conditions following a standard protocol. The positions of the adducts and their relative extent at various positions were determined by fragmentation of the modified oligonucleotides by hot 1 M piperidine and separation, identification, and quantitation of the fragments by the DPAGE method. A Maxam−Gilbert G-lane of the parent oligonucleotide helped to identify the fragments. The results are shown in the form of densitometric scans of the gels in Figure 6. Alkylation of the 3′-G in the 5′-GGN sequences (N = A, T, or G) was approximately 6-fold enhanced compared to alkylation of the 5′-G. In the case of N = C, however, this enhancement was diminished. This exception nonwithholding, the enhanced reactivity of the 3′-Gs was further highlighted by the results at the 5′-GGG sequence (**10**): Both the second and third Gs are highly enhanced sites of the 2,7-DAM adduct, as compared to the 5′-terminal G residue of the sequence. The requirement of a 5′-G neighbor for efficient alkylation of G by 2,7-DAM has been previously demonstrated qualitatively in two laboratories, using restriction fragments (*26*) and synthetic oligo- and polynucleotides (*15*), respectively, as substrates.

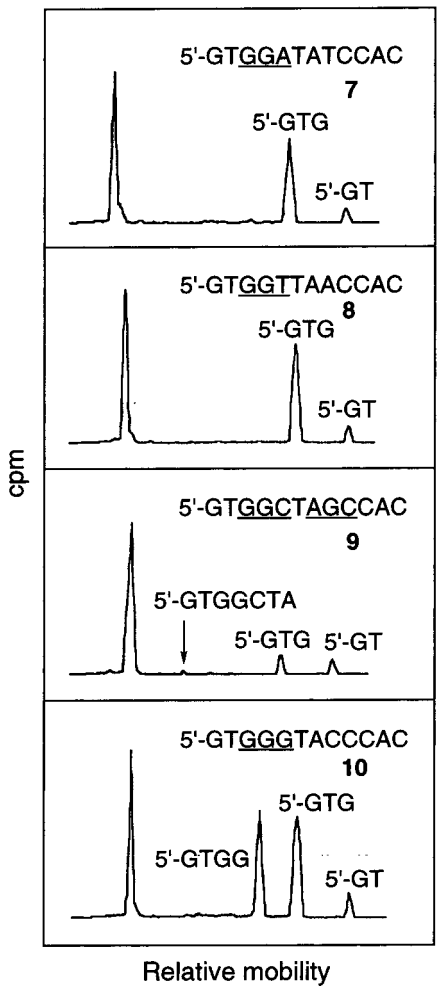

FIGURE 6: Gel electrophoretic fragmentation patterns resulting from guanine-N7 alkylation of self-complementary oligonucleotides **7**−**10** by 2,7-DAM. NGN sequences are underlined. ^{32}P-Labeled oligonucleotides (2 mM) were reacted with 2,7-DAM (1 mM) by activation with H_2/PtO_2 at pH 5.8. After purification, the crude mixtures of 2,7-DAM-modified and unmodified oligonucleotides were heated in 1 M piperidine and analyzed by 20% DPAGE. Quantification was performed by phosphorimagery. Electrophoretic mobility increases to the right. **7**−**10** denote the parent, unmodified oligonucleotides. The fragments generated in the reaction with 2,7-DAM were identified by the matching fragments obtained in the Maxam−Gilbert G-lane of the parent oligonucleotide.

DISCUSSION

*Comparison of the Guanine-N7 Monoadduct of 2,7-DAM (**4**) to the Guanine-N^2 Monoadduct of MC.* The structure of the 2,7-DAM monoadduct of guanine (**4**) is remarkably different from the monoadduct of mitomycin C with guanine (**S2**). Mitomycin C forms a monoadduct at its C1 aziridine position with the N^2 position of guanine in the minor groove (**S2**) with 5′-CG sequence specificity where the 3′-G is the reactive site. An NMR-based structure for this adduct in a 9-mer oligonucleotide duplex (*13*) showed that the drug is oriented in the minor groove with the pyrroloindole quinone ring system pointed toward the 5′ neighbor C and the carbamate moiety of mitomycin C forming a specific H-bond with the exocyclic amino protons of guanine in the opposite strand (Figure 7A). In contrast, in 2,7-DAM, the covalently reacting site is at the C10″ carbamate which changes the covalent modification site from N^2 of guanine in the minor groove to N7 of guanine in the major groove. In the present study we found that the pyrroloindole quinone ring system of 2,7-DAM is oriented 3′ to the adducted guanine (Figure 7B), which is quite opposite to that of the structure of mitomycin C monoadduct (Figure 7A).

Mechanism. A guanine-N7 monoadduct of mitomycin C (**S8**) is formed in trace amounts at G-N7 in DNA; its low yield was attributed to steric hindrance to a direct link between the rigid C1 ring position of MC and the endocyclic guanine-N7 atom (*27*). In contrast, 2,7-DAM is linked to G-N7 by its flexible, unsubstituted C10″-methylene, a primary carbon, and therefore no steric clash prevents

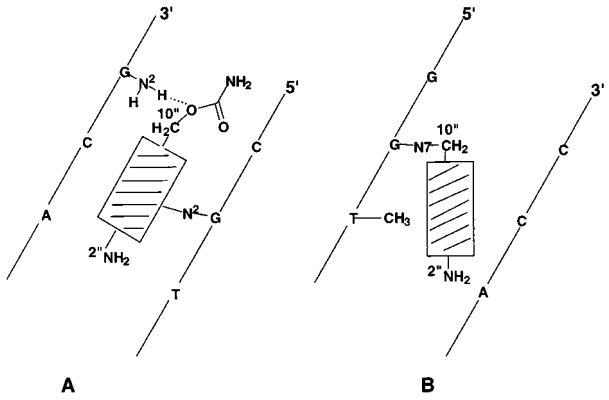

FIGURE 7: Schematic illustration of the alignment of (A) the MC−guanine-N^2 monoadduct in the minor groove and (B) the 2,7-DAM−guanine-N7 adduct in the major groove.

formation of adduct **4** in duplex DNA. It is also notable that the 2,7-DAM−G-N7 adduct **4** is much more stable than the MC−G-N7 adduct (**S8**). In contrast to the latter (*27*), no FAPY derivatives or depurination products of the 2,7-DAM adduct are formed at room temperature and neutral pH (*15*). FAPY formation in **S8** was attributed to neighboring group assistance by 2″-NH_2 of the mitomycin C residue (*27*) which is lacking in the case of adduct **4**.

Comparison of 2,7-DAM to Other Natural Products Which Alkylate DNA at Guanine-N7. The 2,7-DAM−DNA complex represents the first example in which a natural DNA-alkylating agent is aligned in the major groove of DNA in the covalent complex. Although a variety of antibiotics with antitumor or carcinogenic activity are known to alkylate G-N7 in the major groove, the aromatic moiety of such drugs is usually intercalated between two base pairs in the alkylated complex. Examples of this are aflatoxin (*17*, *28*), sterigmatocystin (*18*), kapurimycin (*29*), altromycin (*30*), and the pluramycins (*31*). Major groove alkylation by polycyclic aromatic hydrocarbon diol epoxides at adenine-N^6 also leads to intercalated structures (*32*, *33*). Evidence for intercalation-based structures and alkylation mechanisms of these drugs has been provided by elucidation of the structure of the covalent drug−DNA complexes by NMR. In contrast, the mitosene adduct **4** in modified duplex **5** is evidently more stable in the major groove aligned conformation than in an intercalated one, although free 2,7-DAM binds intercalatively to DNA, with moderate affinity (*34*).

The study of thermal stability of the 2,7-DAM−DNA duplex **5** (Figure S6, Supporting Information, and Table 3) reveals properties of adduct duplex **5** strikingly similar to those of duplexes containing simpler nonintercalating guanine-N7 alkyl groups: lower thermal stability and a more favorable enthalpy but much less favorable entropy in the duplex state, relative to the nonadducted parent duplexes (*24*, *25*). On the other hand, the guanine-N7−aflatoxin B_1 adduct, in which the drug moiety is intercalated, shows increased thermal stability, characteristic of intercalated adducts (*35*). A structural feature of the adduct duplex **5**, namely, confinement of the G-N7 (+) electrostatic interaction in the groove of the duplex (Figure 4), is consistent with the observed decrease of transition entropy resulting in decreased thermal stability over that of the parent duplex.

Origin of the Sequence Selectivity of DNA Alkylation by 2,7-DAM. The solution structure of the 2,7-DAM−DNA complex helps now to understand the observed sequence selectivity of alkylation by 2,7-DAM. Earlier we found that the yield of adduct **4** per G residue was 10-fold greater in poly(dG)·poly(dC) than in poly(dG-dC)·poly(dG-dC). Furthermore, in an oligonucleotide series containing a $(G)_n$ sequence the average yield of **4** per G residue increased as *n* increased from 1 to 4. Two adjacent Gs appeared to be a minimum requirement for the formation of detectable levels of adducts (*15*). A similar sequence selectivity was seen in the reaction of 2,7-DAM with restriction fragments using sequencing gel methodology (*26*). The selectivity is strikingly similar to that of synthetic antitumor alkylating agents such as N-mustards, alkylnitrosamines, and alkylnitrosoureas. These latter agents were shown by Kohn and co-workers (*36*) to react selectively with guanines in DNA which are located in the interior of $(G)_n$ runs. The selectivity patterns correlated with the sequence-dependent negative molecular electrostatic potential (MEP) values of nucleotide residues in the major groove of duplex B-DNA, previously determined by computation by Pullmann and Pullman (*37*). Guanine-N7 sites have the highest negative MEP, and the exact magnitude of this property is sequence-dependent. For example, guanines surrounded by other guanines exhibit more negative MEP minima at N7 than single guanines. Correlation between MEP and G-N7 alkylation intensity was observed only for positively charged reactive species; the neutrally reactive agent dimethyl sulfate shows no sequence selectivity in its alkylation of guanine-N7 (*36*, *37*). However, since the reactive form of 2,7-DAM is protonated on the 10-carbamate leaving group, i.e., it is positively charged (*15*), alkylation by this agent could be subject to MEP-correlated reactivity. Indeed, it is shown here (Figure 8) that the relative extent of alkylation of the individual guanines by 2,7-DAM in the oligonucleotide series **7**−**10** correlates reasonably well with the calculated (*37*) MEP values of their N7 positions. Thus, 2,7-DAM bears all the hallmarks of MEP-directed synthetic alkylating agents of DNA.

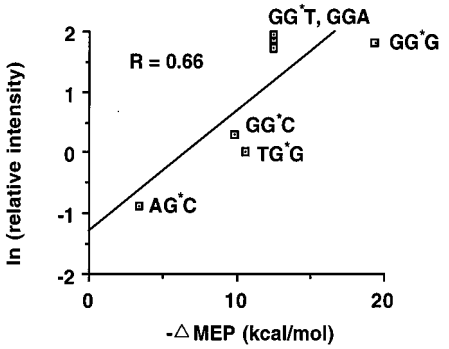

FIGURE 8: Correlation of the intensity of alkylation of guanines by 2,7-DAM in the oligonucleotide series **7**−**10** with the calculated negative molecular electrostatic potential (MEP) of guanine-N7 in 5′-NG*N triplets. The latter values were calculated by summing the MEP values of two overlapping doublets, given in ref *37*. Relative intensity is defined as the ratio of cleavage at G_n relative to cleavage at G_1 in the 5′-$TG_1G_2N_3$ sequence in the oligonucleotide series **7**−**10** (see Figure 2). These ratios were determined using the phosphorimagery data displayed in Figure 2.

2,7-DAM, however, is a natural product, and as such, it has a more complex structure, incorporating a near-planar pyrroloindole quinone system and a number of functional groups. DNA alkylation selectivity of natural products in the major groove does not usually conform simply to the pattern of MEP. In most (if not all) known instances, the covalent reaction is preceded by intercalation into DNA, creating the necessary juxtaposition of the drug's reactive electrophilic center and a guanine-N7 function. Opportunity for a productive juxtaposition is determined by noncovalent interactions between drug and DNA rather than by the MEP (*29*−*31*, *35*). In contrast, the structure of the 2,7-DAM−DNA

[2] Recent studies of the sequence dependence of the reactivity of DNA revealed that the HOMO of a stacked 5′-GG sequence is especially high in energy and is concentrated on the 5′-G (*38*−*40*). As a consequence, one-electron oxidation is favored at the 5′-G of a 5′ -GG stack, in contrast to the nucleophilic substitutions described here, which are favored at the 3′-G. It is clear that the types and sequence selectivities of reactions controlled by MEP are distinct from those controlled by the HOMO.

[3] Decarbamoyl-MC was shown to alkylate DNA in vivo (EMT6 mouse mammary tumor cells) to give adduct **S1** and its 1″-β isomer (M. Tomasz et al., manuscript in preparation).

complex **5,** elucidated here by NMR, reveals that 2,7-DAM is not intercalated; instead, it resides in the major groove, without any apparent sequence-specific noncovalent interaction between the drug and DNA. This unprecedented, sequence-insensitive alignment of a complex aromatic DNA-reactive molecule explains why the sequence selectivity of alkylation by 2,7-DAM, in contrast to other natural products, is determined by the reactivity of DNA alone, directed by the intrinsic sequence-dependent negative MEP at the various guanine-N7 positions in the major groove.[2]

Structure and Biological Activity. Recent studies of the cytotoxicity of MC, 2,7-DAM, and 10-decarbamoyl-MC in mouse mammary tumor cells indicated that 2,7-DAM was much less cytotoxic than MC (*14*) and DMC (*41*). Furthermore, 2,7-DAM is not appreciably mutagenic (M. Tomasz, unpublished results). Thus it was concluded that metabolic formation of 2,7-DAM from MC in the cell represents a detoxification pathway (*14*). The relatively low toxicity of 2,7-DAM is surprising, considering that comparable levels of intracellular alkylation of DNA were observed by all three drugs (*16*). The large difference between the cytotoxicities of 2,7-DAM and MC cannot be explained solely on the basis of the unique cross-linking activity of MC, since decarbamoyl-MC (**3**), which, like 2,7-DAM, is monofunctional, is nevertheless more cytotoxic than 2,7-DAM.[3] The low cytotoxicity of 2,7-DAM contrasts also with the high toxicity and/or mutagenicity observed of covalent major groove-linked drugs which intercalate, e.g., aflatoxin (*42*). A significant factor in the relative biological innocuity of the 2,7-DAM may thus be the unusual, major groove-aligned structure of 2,7-DAM adduct **4**, revealed in the present work. Such structure may be subject to a more facile repair process or an easier, nonmutagenic bypass by polymerases than the minor groove-aligned MC adducts or major groove-intercalated alkylators. The well-defined, relatively simple structure of the 2,7-DAM adduct makes it an attractive model to use for investigating these possibilities.

ACKNOWLEDGMENT

We thank Dr. Dinesh M. Vyas, Bristol-Myers Squibb Co., Wallingford, CT, for providing us with mitomycin C.

SUPPORTING INFORMATION AVAILABLE

Details of the thermodynamic analysis of the melting curves, two charts (chemical structures of **S1**−**S4** and **S8**), two schemes (formation of adduct **4** from **1** and deribosylation of **4** to **S7**), two tables for adduct duplex **5** (proton chemical shifts and selective helical parameters), and six figures of one-dimensional NMR spectra, a NOESY plot, a TOCSY plot, a NOESY and COSY plot, helical parameters (sugar pucker, chi, *X*-displacement, *Y*-displacement, twist, and rise), and thermal melting curves. This material is available free of charge via the Internet at http://pubs.acs.org.

REFERENCES

1. Hata, T., Sano, Y., Sugawara, R., Matsumae, A., Kanamorei, K., Shima, T., and Hoshi, T. (1956) *J. Antibiot., Ser. A 9*, 141−146.
2. Verweij, J., and Pinedo, H. (1990) in *Cancer chemotherapy and biological modifiers, Annual 11* (Pinedo, H. M., Chabner, B. A., and Longo, D. L., Eds.) pp 67−73, Elsevier Science Publishers B.V., Amsterdam.
3. Chirrey, L., Cummings, J., Halbert, G. W., and Smyth, J. F. (1995) *Cancer Chemother. Pharmacol. 35*, 318−322.
4. Lipman, R., and Tomasz, M. (1981) *Biochemistry 20*, 5056−5061.
5. Iyer, V. N., and Szybalski, W. (1963) *Proc. Natl. Acad. Sci. U.S.A. 60*, 355−362.
6. Tomasz, M. (1994) in *Molecular Aspects of Anticancer Drug−DNA Interactions* (Neidle, S., and Waring, M., Eds.) Vol. 2, pp 312−349, Macmillan, London, and CRC Press, Fort Lauderdale, FL.
7. Li, V., and Kohn, H. (1991) *J. Am. Chem. Soc. 113*, 275−283.
8. Kumar, S., Lipman, R., and Tomasz, M. (1992) *Biochemistry 31*, 1399−1407.
9. Teng, S. P., Woodson, S. A., and Crothers, D. M. (1989) *Biochemistry 28*, 3901−3907.
10. Weidner, M. F., Millard, J. T., and Hopkins, P. B. (1989) *J. Am. Chem. Soc. 111*, 9270−9272.
11. Borowy-Borowski, H., Lipman, R., and Tomasz, M. (1990) *Biochemistry 29*, 2999−3004.
12. Norman, D., Live, D., Sastry, M., Lipman, R., Hingerty, B. E., Tomasz, M., Broyde, S., and Patel, D. J. (1990) *Biochemistry 29*, 2861−2876.
13. Sastry, M., Fiala, R., Lipman, R., Tomasz, M., and Patel, D. J. (1995) *J. Mol. Biol. 247*, 338−359.
14. Palom, Y., Belcourt, M. F., Suresh Kumar, G., Arai, H., Kasai, M., Sartorelli, A. C., Rockwell, S., and Tomasz, M. (1998) *Oncology Res. 10*, 509−521.
15. Suresh Kumar, G., Musser, S. M., Cummings, J., and Tomasz, M. (1996) *J. Am. Chem. Soc. 118*, 9209−9217.
16. Palom, Y., Belcourt, M. F., Tang, L.-Q., Mehta, S. S., Sartorelli, A. C., Pritsos, C. A., Pritsos, K. L., Rockwell, S., and Tomasz, M. (2001) *Biochem. Pharmacol. 61*, 1519−1531.
17. Gopalakrishnan, S., Harris, T. M., and Stone, M. P. (1990) *Biochemistry 29*, 10438−10448.
18. Gopalakrishnan, S., Liu, X., and Patel, D. J. (1992) *Biochemistry 31*, 10790−10801.
19. Gargiulo, D., Musser, S. S., Yang, L., Fukuyama, T., and Tomasz, M. (1995) *J. Am Chem. Soc. 117*, 9388−9398.
20. Puglisi, J. D., and Tinoco, I., Jr. (1989) *Methods Enzymol. 180*, 304−325.
21. Plateau, P., and Gueron, M. (1982) *J. Am. Chem. Soc. 104*, 7310−7311.
22. Gopalakrishnan, S., Stone, M. P., and Harris, T. M. (1989) *J. Am. Chem. Soc. 111*, 7232−7239.
23. Singer, B., and Grunberger, D. (1983) *Molecular Biology of Mutagens and Carcinogens*, pp 15−44, Plenum Press, New York.
24. Persmark, M., and Guengerich, F. P. (1994) *Biochemistry 33*, 8662−8672.
25. Ezaz-Nikpay, K., and Verdine, G. L. (1992) *J. Am. Chem. Soc. 114*, 6562−6564.
26. Prakash, A. S., Beall, H., Ross, D., and Gibson, N. W. (1993) *Biochemistry 32*, 5518−5525.
27. Tomasz, M., Lipman, R., Lee, M. S., Verdine, G. L., and Nakanishi, K. (1987) *Biochemistry 26*, 2010−2027.
28. Iyer, R. S., Coles, B. F., Raney, K. D., Their, R., Guengerich, F. P., and Harris, T. M. (1994) *J. Am. Chem Soc. 116*, 1603−1609.
29. Nakatani, K., Okamoto, A., Matsuno, T., and Saito, I. (1998) *J. Am. Chem. Soc. 120*, 11219−11225.
30. Hansen, M., and Hurley, L. H. (1995) *J. Am Chem. Soc. 117*, 2421−2429.
31. Sun, D., Hansen, M., and Hurley, L. H. (1995) *J. Am Chem. Soc. 117*, 2430−2440.
32. Cosman, M., Fiala, R., Hingerty, B. E., Laryea, A., Lee, H., Harvey, R. G., Amin, S., Geacintov, N. E., Broyde, S., and Patel, D. J. (1993) *Biochemistry 32*, 12488−12497.

33. Zegar, I. S., Kim, S. J., Johansen, T. N., Horton, P. J., Harris, C. M., Harris, T. M., and Stone, M. P. (1996) *Biochemistry 35*, 6212−6224.
34. Suresh Kumar, G., He, Q.-Y., Behr-Ventura, D., and Tomasz, M. (1995) *Biochemistry 34*, 2662−2671.
35. Stone, M. P., Gopalakrishnan, S., Raney, K. D., Raney, V. M., Byrd, S., and Harris, T. M. (1990) in Molecular Basis of Specificity in Nucleic Acid−Drug Interactions, *The Jerusalem Symposia on Quantum Chemistry and Biochemistry* (Pullman, B., and Jortner, J., Eds.) Vol. 23, pp 452−480, Kluwer Academic Publishers, Amsterdam, The Netherlands.
36. Kohn, K. W., Hartley, J. A., and Mattes, W. B. (1987) *Nucleic Acids Res. 14*, 10531−10549.
37. Pullman, A., and Pullman, B. (1981) *Q. Rev. Biophys. 14*, 289−380.
38. Saito, I., Nakamura, T., Nakatani, K., Yoshioka, Y., Yamaguchi, K., and Sugiyama, H. (1998) *J. Am. Chem. Soc. 120*, 12686−12687.
39. Prat, F., Houk, K. N., and Foote, C. S. (1998) *J. Am Chem. Soc. 120*, 12686−12687.
40. Saito, I., Nakamura, T., and Nakatani, K. (2000) *J. Am. Chem. Soc. 122*, 3001−3006.
41. Kim, S. Y., and Rockwell, S. (1995) *Oncology Res. 7*, 39−47.
42. Busby, W. F., and Wogan, G. N. (1984) in *Chemical Carcinogens* (Searle, C. E., Ed.) 2nd ed., pp 945−1036, American Chemical Society, Washington, DC.

BI010965A